

# Triaxial deformation in $^{10}\text{Be}$

*N. Itagaki,<sup>1\*</sup> S. Hirose,<sup>1</sup> T. Otsuka,<sup>1,2</sup> S. Okabe,<sup>3</sup> and K. Ikeda<sup>2</sup>*

<sup>1</sup> *Department of physics, University of Tokyo, Hongo, Tokyo 113-0033, Japan*

<sup>2</sup> *The Institute of Physical and Chemical Research (RIKEN), Wako, Saitama 351-0198, Japan*

<sup>3</sup> *Center for Information and Multimedia Studies, Hokkaido University, Sapporo 060-0810, Japan*

## Abstract

The triaxial deformation in  $^{10}\text{Be}$  is investigated using a microscopic  $\alpha+\alpha+n+n$  model. The states of two valence neutrons are classified based on the molecular-orbit (MO) model, and the  $\pi$ -orbit is introduced about the axis connecting the two  $\alpha$ -clusters for the description of the rotational bands. There appear two rotational bands comprised mainly of  $K^\pi = 0^+$  and  $K^\pi = 2^+$ , respectively, at low excitation energy, where the two valence neutrons occupy  $K^\pi = 3/2^-$  or  $K^\pi = 1/2^-$  orbits. The triaxiality and the  $K$ -mixing are discussed in connection to the molecular structure, particularly, to the spin-orbit splitting. The extent of the triaxial deformation is evaluated in terms of the electro-magnetic transition matrix elements (Davydov-Filippov model,  $Q$ -invariant model), and density distribution in the intrinsic frame. The obtained values turned out to be  $\gamma = 15^\circ \sim 20^\circ$ .

PACS number(s): 21.10.-k, 21.60.Gx

## I. INTRODUCTION

Recently, exotic structures of the Be isotopes have been theoretically and experimentally studied, and many new phenomena have been discussed [1–7]. One of them is the appearance of the cluster rotational band structure in the excited states of  $^{10}\text{Be}$  ( $\alpha+^6\text{He}$ ) [5,7] and  $^{12}\text{Be}$  ( $\alpha+^8\text{He}$ ,  $^6\text{He}+^6\text{He}$ ) [4,6]. We have suggested [8–10], based on the molecular-orbit (MO) model, that the development of  $\alpha$ - $\alpha$  cluster structure depends on the neutron orbits located around the core comprised of  $\alpha$ -clusters. In the second  $0^+$  state of  $^{10}\text{Be}$ , an anomalously prolonged  $\alpha$ - $\alpha$  clustering structure emerges due to the valence neutrons located along the  $\alpha$ - $\alpha$  axis [8,9].

The nucleus  $^{10}\text{Be}$  has been known to have a strong  $\beta$  deformation due to the  $\alpha$ - $\alpha$  core. In this paper, we discuss another aspect, a triaxial deformation. The triaxial deformation is possible as a result of the dynamics of the two valence neutrons. The triaxiality of  $^{10}\text{Be}$

---

\*E-mail: itagaki@phys.s.u-tokyo.ac.jp

has been theoretically discussed based on the deformed oscillator model [11], in which a  $\gamma$  distortion of  $34.8^\circ$  has been predicted. According to Davydov-Filippov model [12], this  $\gamma$  value suggests that the excitation energy of the second  $2^+$  state is 2.3 times higher than that of the first  $2^+$  state. In  $^{10}\text{Be}$ , the first  $2^+$  state is observed at 3.358 MeV, and several  $2^+$  states have been observed around 8 MeV region. Because of the presence of the  $2^+$  states in this energy region, recently, an experimental study has been performed in order to identify a triaxial structure of  $^{10}\text{Be}$  [13].

In this paper, we discuss the triaxiality of  $^{10}\text{Be}$  as a composite system of the  $\alpha$ - $\alpha$  core and two valence neutrons, comparing with other theoretical models. In our previous study on  $^{10}\text{Be}$  [8], all of the observed low-lying positive- and negative-parity states are explained as combinations of three basic orbits ( $K^\pi = 3/2^-, 1/2^+$ , and  $1/2^-$ ) of two valence neutrons around the two  $\alpha$ -clusters. Here, the  $z$ -axis is taken to be the axis connecting two  $\alpha$ -clusters. If we adopt  $K^\pi = 3/2^-$  or  $1/2^-$  orbits for the two valence neutrons, there appear two rotational bands in low energy; one is dominated by the  $K = 0$  intrinsic structure and the other by  $K = 2$ . The calculated two  $2^+$  states of these bands can be related to the observed first  $2^+$  state at 3.358 MeV and the second  $2^+$  state at 5.958 MeV. It is therefore important to show how the triaxial intrinsic configuration emerges in these states, and how the orbits of the valence neutrons deviate from the axial symmetry. Here, we calculate the electromagnetic transition between these  $K = 0$  and  $K = 2$  bands (B(E2:  $K = 2 \rightarrow K = 0$ )) as a signal of a triaxial deformation. This transition is suppressed when the orbitals are of pure axial symmetry. However, the orbitals may deviate from the axial symmetry, when the valence neutrons are mutually more correlated and form a localized di-neutron pair due to the neutron-neutron interaction. The recoil effect of the valence neutrons with respect to the  $\alpha$ - $\alpha$  core then plays a role to break the axial symmetry of the charge distribution.

This paper is organized as follows. In section II, we give a description of the single-particle orbits around the two  $\alpha$ -clusters based on MO. In section III, we show our results on  $^{10}\text{Be}$ , and a conclusion is given in section IV.

## II. EXTENDED MOLECULAR-ORBIT MODEL

### A. Wave function of $^{10}\text{Be}$

We introduce a microscopic  $\alpha+\alpha+2n$  model for  $^{10}\text{Be}$ . The neutron configurations are introduced based on the molecular orbit (MO) picture [14–16]. The total wave function is fully antisymmetrized and expressed as a superposition of Slater determinants with various configurations of the valence neutrons. The Slater determinants are also superposed with respect to different relative distances between the two  $\alpha$  clusters ( $d$ ). The projection to the eigen states of angular momentum  $J$  is numerically performed. All nucleons are described by Gaussians with a common oscillator parameter  $s = \frac{1}{\sqrt{2\nu}}$  set equal to 1.46 fm. The  $\alpha$  cluster located at  $R_\alpha$  on the  $z$ -axis contains four nucleons.

$$\phi^{(\alpha)} = G_{R_\alpha}^{p\uparrow} G_{R_\alpha}^{p\downarrow} G_{R_\alpha}^{n\uparrow} G_{R_\alpha}^{n\downarrow} \chi_{p\uparrow} \chi_{p\downarrow} \chi_{n\uparrow} \chi_{n\downarrow}. \quad (1)$$

Here,  $G$  represents a Gaussian:

$$G_{R_\alpha} = \left(\frac{2\nu}{\pi}\right)^{\frac{3}{4}} \exp[-\nu(\vec{r} - \vec{R}_\alpha)^2], \quad \nu = 1/2s^2, \quad (2)$$

where  $\vec{R}_\alpha = R_\alpha \vec{e}_z$  with  $\vec{e}_z$  being the unit vector pointing the  $z$ -direction. The actual value of  $R_\alpha$  is  $d/2$  or  $-d/2$  in this work. The wave function of the  $i$ -th valence neutron ( $\phi_i \chi_i$ ) is expressed by a linear combination of local Gaussians:

$$\phi_i \chi_i = \sum_j g_j G_{R_j} \chi_i, \quad (3)$$

$$G_{R_j} = \left( \frac{2\nu}{\pi} \right)^{\frac{3}{4}} \exp[-\nu(\vec{r}_i - \vec{R}_j)^2], \quad (4)$$

where  $\vec{R}_j$  is a parameter corresponding to the Gaussian center.

The two valence neutrons are classified according to the MO picture. In the MO model, the states of the valence neutrons are expressed by a linear combination of orbits around two  $\alpha$  clusters. Here, we notice that the valence neutrons and the neutrons in the  $\alpha$  clusters are identical particles, and the valence neutrons must be orthogonal to the forbidden space due to the  $\alpha$ - $\alpha$  core. The lowest orbit then has one node and negative parity, that is the  $p$ -orbit. We take the harmonic-oscillator-type wave function for the  $p$ -orbit. Such  $p$ -orbits in the  $x$ -,  $y$ -, and  $z$ -direction are denoted as  $\psi_x$ ,  $\psi_y$ , and  $\psi_z$ , respectively. We now classify single particle orbits for the valence neutrons in terms of  $K$  quantum numbers:

$$\psi_x + i\psi_y = (x + iy) \exp[-\nu r^2] \propto r Y_{11} \exp[-\nu r^2], \quad (5)$$

$$\psi_z = z \exp[-\nu r^2] \propto r Y_{10} \exp[-\nu r^2], \quad (6)$$

$$\psi_x - i\psi_y = (x - iy) \exp[-\nu r^2] \propto r Y_{1-1} \exp[-\nu r^2]. \quad (7)$$

These  $p$ -orbits have  $K = 1, 0$ , and  $-1$ , respectively. Here,  $x$ ,  $y$ , and  $z$  are relative to  $\vec{R}_\alpha$ .

Now we construct MO from these  $p$ -orbits. Since each valence neutron can move around one of the two  $\alpha$ -clusters, there should be two sets of the  $p$ -orbits defined with respect to those two  $\alpha$ -clusters. Thus, the  $(\psi_x \pm i\psi_y)$  orbit whose center is shifted at  $+a$  ( $-a$ ) on the  $z$ -axis is denoted as  $(\psi_x \pm i\psi_y)_{+a}$  ( $(\psi_x \pm i\psi_y)_{-a}$ ). As linear combinations of these orbits, the lowest MOs are expressed as:

$$\psi_1^{MO} = (\psi_x + i\psi_y)_{+a} + (\psi_x + i\psi_y)_{-a}, \quad (8)$$

$$\psi_{-1}^{MO} = (\psi_x - i\psi_y)_{+a} + (\psi_x - i\psi_y)_{-a}. \quad (9)$$

These orbits clearly have  $K = 1$  and  $K = -1$ , respectively. In these cases, the classical picture of  $p$ -orbit is a circular motion about the  $\alpha$ - $\alpha$  ( $z$ ) axis. This is the so-called  $\pi$ -orbit.

If we take a linear combination of  $(\psi_z)_{+a}$  and  $(\psi_z)_{-a}$ , the orbit becomes the so-called  $\sigma$ -orbit, just along the  $\alpha$ - $\alpha$  ( $z$ ) axis. This orbit is a higher-nodal orbit and only relevant to the second  $0^+$  state, discussed also in antisymmetrized molecular dynamics (AMD) calculations [17] and in stochastic variational method (SVM) calculations [18], and now we disregard this orbit.

These  $(\psi_x)_{+a}$ ,  $(\psi_x)_{-a}$ ,  $(\psi_y)_{+a}$ , and  $(\psi_y)_{-a}$  orbits can be approximated by a combination of two local Gaussians, whose centers are shifted by a variational parameter  $b$  perpendicular to the  $z$ -axis. We thus use the following wave functions,

$$(\psi_x)_{+a} \propto G_{a\bar{e}_z+b\bar{e}_x} - G_{a\bar{e}_z-b\bar{e}_x}, \quad (\psi_y)_{+a} \propto G_{a\bar{e}_z+b\bar{e}_y} - G_{a\bar{e}_z-b\bar{e}_y}, \quad \dots \quad (10)$$

The values of these parameters  $a$  and  $b$  are variationally determined by using the cooling method in AMD [19–23] independently for each  $\alpha$ - $\alpha$  distance. Since the rotational symmetry about the  $z$ -axis is broken with Eq. (10), the wave functions do not have exactly conserved quantum number  $K$ . On the other hand, the parameter  $b$  is small enough usually, and the  $K^\pi$  number is preserved to a good extent, and is expressed hereafter as  $\bar{K}^\pi$ .

When these orbital part of the wave functions are coupled with the spin part, the orbits with  $\bar{K}^\pi = 3/2, 1/2, -1/2$ , and  $-3/2$  are introduced, as follows:

$$|3/2^-\rangle = \psi_1^{MO}|n \uparrow\rangle, \quad |1/2^-\rangle = \psi_1^{MO}|n \downarrow\rangle, \quad (11)$$

and their time reversal,

$$|-3/2^-\rangle = \psi_{-1}^{MO}|n \downarrow\rangle, \quad |-1/2^-\rangle = \psi_{-1}^{MO}|n \uparrow\rangle. \quad (12)$$

## B. Hamiltonian

The Hamiltonian consists of the kinetic energy term, the central two-body interaction term, the two-body spin-orbit interaction term, and the Coulomb interaction term:

$$\mathcal{H} = \sum_i T_i - T_{cm} + \sum_{i<j} V_{ij} + \sum_{i<j} V_{ij}^{ls} + \sum_{i<j} \frac{e^2}{4r_{ij}} (1 - \tau_z^i)(1 - \tau_z^j). \quad (13)$$

The effective nucleon-nucleon interactions are Volkov No.2 [24] for the central part and the G3RS spin-orbit term [25] for the spin-orbit part, as follows:

$$V_{ij} = \{V_1 e^{-a_1 r_{ij}^2} + V_2 e^{-a_2 r_{ij}^2}\} \{W - MP^\sigma P^\tau + BP^\sigma - HP^\tau\}, \quad (14)$$

$$V_{ij}^{ls} = V_0^{ls} \{e^{-a_1 r_{ij}^2} - e^{-a_2 r_{ij}^2}\} \vec{L} \cdot \vec{S} P_{31}, \quad (15)$$

where  $P_{31}$  is a projection operator onto the triplet odd state, and  $\vec{L}$  and  $\vec{S}$  operators represent the relative angular momentum and total spin of the interacting two nucleons, respectively. The parameters are  $V_1 = -60.650$  MeV,  $V_2 = 61.140$  MeV,  $a_1 = 0.309$  fm<sup>-2</sup> and  $a_2 = 0.980$  fm<sup>-2</sup> for the central interaction, and  $V_0^{ls} = 2000$  MeV,  $a_1 = 5.00$  fm<sup>-2</sup>, and  $a_2 = 2.778$  fm<sup>-2</sup> for the spin-orbit interaction. We employ the Majorana exchange parameter  $M = 0.6$  ( $W = 0.4$ ), the Bartlett exchange parameter  $B = 0.125$  and the Heisenberg exchange parameter  $H = 0.125$  for the Volkov interaction (using  $B$  and  $H$ , there is no neutron-neutron bound state). All these parameters are determined from  $\alpha + n$  and  $\alpha + \alpha$  scattering phase shifts and the binding energy of the deuteron [26].

### C. Configurations of the valence neutrons

For  $^{10}\text{Be}$ , we introduce three configurations of  $\Phi((3/2^-)^2)$ ,  $\Phi((1/2^-)^2)$ , and  $\Phi(3/2^- 1/2^-)$  for the two valence neutrons, and mixing amplitude of these configurations are variationally determined after the angular momentum projection.

It will be shown that the  $\Phi((3/2^-)^2)$  configuration, where valence neutrons occupy orbits with  $\bar{K}^\pi = 3/2^-$  and  $\bar{K}^\pi = -3/2^-$  is the main component of the ground state. The energy shift due to the spin-orbit interaction acting effectively on a valence neutron is proportional to  $-\langle \vec{l} \cdot \vec{s} \rangle$ . It is, therefore, favored that the orbital part and the spin part of  $\bar{K}$  are coupled to be parallel. This means that the spin-up valence neutron ( $|n \uparrow\rangle$ ) has  $\bar{K}^\pi = 3/2^-$ , while the spin-down valence neutron ( $|n \downarrow\rangle$ )  $\bar{K}^\pi = -3/2^-$ , giving rise to the wave function of the two valence neutrons:

$$\Phi((3/2^-)^2) = \mathcal{A}[\phi_1^{(\alpha)} \phi_2^{(\alpha)} (\phi_{c1} \chi_{c1}) (\phi_{c2} \chi_{c2})], \quad (16)$$

with

$$\phi_{c1} \chi_{c1} = \psi_1^{MO} |n \uparrow\rangle, \quad \phi_{c2} \chi_{c2} = \psi_{-1}^{MO} |n \downarrow\rangle. \quad (17)$$

We also introduce a basis state  $\Phi((1/2^-)^2)$ , which the spin-orbit interaction does not favor. They are defined by flipping the spin-part of the  $3/2^-$  and  $-3/2^-$  wave functions. and the valence neutrons occupy orbits of  $\bar{K}^\pi = 1/2^-$  and  $\bar{K}^\pi = -1/2^-$ :

$$\phi_{c1} \chi_{c1} = \psi_1^{MO} |n \downarrow\rangle, \quad \phi_{c2} \chi_{c2} = \psi_{-1}^{MO} |n \uparrow\rangle. \quad (18)$$

The  $\Phi(3/2^- 1/2^-)$  configuration with  $\bar{K} = 2$  is constructed as a combination of the valence neutrons in the  $\bar{K}^\pi = 3/2^-$  and  $\bar{K}^\pi = 1/2^-$  orbits.

$$\phi_{c1} \chi_{c1} = \psi_1^{MO} |n \uparrow\rangle, \quad \phi_{c2} \chi_{c2} = \psi_1^{MO} |n \downarrow\rangle. \quad (19)$$

### III. TRIAXIAL STRUCTURE IN $^{10}\text{BE}$

In  $^{10}\text{Be}$ , we adopt three configurations  $\Phi((3/2^-)^2)$ ,  $\Phi((1/2^-)^2)$ , and  $\Phi(3/2^- 1/2^-)$ , where single particle orbits with  $\bar{K} = 3/2^-, 1/2^-$  have been introduced. The values of the parameters for the valence neutrons are obtained variationally. The parameter  $a$  describes the positions of the Gaussian centers on the  $\alpha$ - $\alpha$  ( $z$ ) axis, and parameter  $b$  corresponds to the rotation radius of the  $\pi$ -orbit about the  $\alpha$ - $\alpha$  axis. The optimized values are listed in Table I.

---

Table I

---

The parameter  $a$  is obtained to be approximately the same value as  $d/2$ . Therefore, the picture ‘‘orbit around the  $\alpha$ -cluster’’ works well, while there is a small deviation of the orbit along the  $z$ -axis. The parameter  $b$  depends on the configurations. For  $\Phi((3/2^-)^2)$ ,  $b$  appears

to be  $\sim 1$  fm. For  $\Phi((1/2^-)^2)$ ,  $b$  becomes longer as being 2 fm, since the spin-orbit interaction acts attractively for  $\Phi((3/2^-)^2)$  whereas repulsively for  $\Phi((1/2^-)^2)$ .

Before performing the angular momentum projection, we discuss the triaxial deformation of the intrinsic wave function. The intrinsic density of  $\Phi((3/2^-)^2)$  is shown in Fig. 1 ((a):  $xz$ -plane, (b):  $xy$ -plane), where the  $\alpha$ - $\alpha$  distance is chosen to be optimal, as it turns out to be 3 fm.

---

Fig. 1 (a), (b)

---

The intrinsic density is defined as a snap-shot of a rotating system. The plane in which the spin-up valence neutrons stays at a given moment is defined as the  $xz$ -plane, with the  $z$ -axis being the  $\alpha$ - $\alpha$  axis. Therefore, the spin-up valence neutron is fixed on the  $xz$ -plane, and the spin-down valence neutrons occupy the normal  $\bar{K} = -3/2^-$  orbit. The intrinsic density on the  $xz$ -plane (Fig.1 (a)) shows a large  $\beta$  deformation along the  $z$ -axis due to the presence of two  $\alpha$ -clusters. As for the  $xy$ -plane (Fig. 1 (b)), the density shows deviation from circular distribution and mixture of a triaxial component is evident. The contour-line of 0.01 in Fig. 1 (a) and (b) suggests the deformation of this nucleus is  $\beta \sim 0.5$  and  $\gamma = 11^\circ$ .

We then perform the angular momentum projection, where the wave function is rotated and integrated over the Euler angle, and the rotational symmetry is restored. Here, the  $K$ -mixing between  $K = 0$  and  $K = 2$  finally determines the degree of the triaxiality of the system.

This intrinsic wave function is numerically projected to the eigen states of angular momentum, and the basis states with parameters listed in Table I are superposed by generator coordinate method (GCM). Here, the coefficients representing linear combinations of Gaussians for each single particle orbit are treated as variational parameters to take into account deviations from the original orbits. Because of this, not only “single-particle” MO state where the valence neutrons independently rotate around the  $\alpha$ - $\alpha$  core, but also more complex states where the valence neutrons are mutually more correlated as a di-neutron cluster can be included.

The energy levels of  $^{10}\text{Be}$  are shown in Fig. 2. Using our framework, the binding energy of one  $\alpha$ -cluster is calculated to be 27.5 MeV, and the threshold energy of free  $\alpha + \alpha + n + n$  system is  $2 \times (-27.5) = -55.0$  MeV. Experimentally, the ground state is lower than this energy by 8.4 MeV.

---

Fig. 2

---

The left and middle columns in Fig. 2 show the calculated energy levels with the constraints of  $K = 0$  and  $K = 2$ , respectively, and the right column shows the result after the  $K$ -mixing. In  $K = 0$  column, it can be seen that the ground  $0^+$  state at  $-60.5$  MeV, the  $2^+$  state at  $-56.9$  MeV, and the  $4^+$  state at  $-47.6$  MeV form a rotational band structure. They fit quite well into the  $J(J+1)$  rule, and the dominant component is  $(3/2^-)^2$  for the two valence neutrons. For  $K = 2$  column, the  $2^+$  state at  $-54.9$  MeV, the  $3^+$  state at  $-51.1$  MeV, and the  $4^+$  state at  $-46.1$  MeV form a rotational band structure. They also fit quite well into

the  $J(J+1)$  rule. The  $K=2$  band dominantly has a component of  $(3/2^-)(1/2^-)$  for the two valence neutrons, where one of them feels the spin-orbit interaction attractively and the other feels repulsively. After the mixing of these two bands, the  $2^+$  state with  $K=0$  at  $-56.9$  MeV becomes  $-57.3$  MeV ( $E_x = 3.1$  MeV, experimentally  $3.358$  MeV), and  $2^+$  state with  $K=2$  is slightly pushed up to  $-54.9$  MeV ( $E_x = 5.6$  MeV, experimentally  $5.958$  MeV). The first  $2^+$  state has the squared overlap with the  $K=0$  state by  $0.96$ , and the second  $2^+$  state has the squared overlap with the  $K=2$  state by  $0.92$ . Therefore, the second  $2^+$  state has the component of  $K=0$  by  $8\%$ , and it can be considered as an indication of a triaxial deformation.

This triaxiality of the  $2^+$  states is reflected in the electro-magnetic transition rate, and  $B(E2)$  values are summarized in Table II.

---

Table II

---

The E2 transition between the first  $2^+$  state and the ground state is calculated as  $B(E2: 2_1^+ \rightarrow 0_1^+) = 11.8 e^2\text{fm}^4$ , which agrees with the experimental value of  $10.04 \pm 1.2 e^2\text{fm}^4$ . Furthermore, the interband transition is calculated:  $B(E2: 2_1^+ \rightarrow 2_2^+) = 3.99 e^2\text{fm}^4$ . If the system is axially symmetric, this transition between different  $K$ -values is more suppressed. Therefore, the value indicates the  $2^+$  states have component of a triaxial deformation.

Using Davydov-Filippov model [12], we can estimate the degree of the triaxiality as a function of the  $\gamma$  angle. The ratios  $\frac{B(E2: 2_2^+ \rightarrow 0_1^+)}{B(E2: 2_1^+ \rightarrow 0_1^+)}$  and  $\frac{B(E2: 2_2^+ \rightarrow 2_1^+)}{B(E2: 2_1^+ \rightarrow 0_1^+)}$  are given in Davydov-Filippov model as follows:

$$\frac{B(E2: 2_2^+ \rightarrow 0_1^+)}{B(E2: 2_1^+ \rightarrow 0_1^+)} = \frac{1 - \frac{3-2\sin^2(3\gamma)}{\sqrt{9-8\sin^2(3\gamma)}}}{1 + \frac{3-2\sin^2(3\gamma)}{\sqrt{9-8\sin^2(3\gamma)}}}, \quad (20)$$

$$\frac{B(E2: 2_2^+ \rightarrow 2_1^+)}{B(E2: 2_1^+ \rightarrow 0_1^+)} = \frac{\frac{20}{7} \frac{\sin^2(3\gamma)}{9-8\sin^2(3\gamma)}}{1 + \frac{3-2\sin^2(3\gamma)}{\sqrt{9-8\sin^2(3\gamma)}}}. \quad (21)$$

These values are compared with our calculation in Fig. 3.

---

Fig. 3

---

The solid line in Fig. 3 shows the ratio  $\frac{B(E2: 2_2^+ \rightarrow 2_1^+)}{B(E2: 2_1^+ \rightarrow 0_1^+)}$  calculated with the Davidov-Filippov model. The ratio becomes  $0.34$  in our calculation, and it has a crossing point with Davydov-Filippov model around  $\gamma = 19^\circ$ . The dotted line in Fig. 3 shows the ratio  $\frac{B(E2: 2_2^+ \rightarrow 0_1^+)}{B(E2: 2_1^+ \rightarrow 0_1^+)}$  calculated with the Davidov-Filippov model, and it crosses with our result of  $0.059$  around  $\gamma = 17^\circ$  and  $22^\circ$ . These results strongly suggest that  $^{10}\text{Be}$  has a triaxial deformation of  $\gamma = 15^\circ \sim 20^\circ$ . Although the  $\alpha$ - $\alpha$  core is of axial symmetry and electric charge are only in the  $\alpha$ 's, the recoil effect gives rise to a change from the axial symmetry to the triaxial shape.

The  $\gamma$ -value can be deduced also in terms of  $Q$ -invariant model. In Ref. [27], the  $\gamma$ -value is related to the reduced matrix elements of  $Q$  operator:

$$q_2 = \sum_i \langle 0_1^+ || Q || 2_i^+ \rangle \langle 2_i^+ || Q || 0_1^+ \rangle, \quad (22)$$

$$q_3 = \sqrt{\frac{7}{10}} \sum_{i,j} \langle 0_1^+ || Q || 2_i^+ \rangle \langle 2_i^+ || Q || 2_j^+ \rangle \langle 2_j^+ || Q || 0_1^+ \rangle, \quad (23)$$

$$\frac{q_3}{q_2^{\frac{3}{2}}} = \cos 3\gamma. \quad (24)$$

Using these relations and taking the sum over indices  $i$  and  $j$  up to 2, our calculated results correspond to  $\gamma = 20.1^\circ$ .

We discuss the electro-magnetic transition between the two  $2^+$  states ( $K$ -mixing effect between the two  $2^+$  states) by artificially changing the strength parameter  $V_0^{ls}$  in Eq. (15) for the spin-orbit term. The Majorana parameter  $M$  for the central term is simultaneously changed to keep the calculated binding energy constant. In Table III, the B(E2:  $2_1^+ \rightarrow 2_2^+$ ) values are listed together with the calculated energies and magnetic dipole moments. Using the original interaction, the B(E2:  $2_1^+ \rightarrow 2_2^+$ ) value is predicted as  $3.99 e^2\text{fm}^4$ .

---

Table III

---

When we increase the  $V_0^{ls}$  value, the excitation energy of the second  $2^+$  state becomes higher, since one of the valence neutrons repulsively feels the spin-orbit interaction. The original interaction ( $V_0^{ls} = 2000$  MeV and  $M = 0.6$ ) gives  $E_x = 5.70$  MeV for the  $2_2^+$  state, but the interaction with  $V_0^{ls} = 2500$  MeV and  $M = 0.61$  gives  $E_x = 6.82$  MeV. The B(E2:  $2_1^+ \rightarrow 2_2^+$ ) value then decreases from  $3.99 e^2\text{fm}^4$  to  $2.20 e^2\text{fm}^4$ . Therefore, it is considered that with increasing  $LS$  strength, the  $K$  quantum number of each  $2^+$  state approaches to a good number, where the E2 transition between the two  $2^+$  states is suppressed. On the other hand, when the spin-orbit interaction becomes weaker, the transition rapidly increases. The  $V_0^{ls}$  value of 1500 MeV gives the B(E2:  $2_1^+ \rightarrow 2_2^+$ ) values of  $9.53 e^2\text{fm}^4$ , and when we adopt  $V_0^{ls} = 1000$  MeV, the value becomes  $17.53 e^2\text{fm}^4$ . Here, the orbits of the valence neutrons deviate from ones with good  $K$  quantum numbers, and a triaxial  $\alpha+\alpha$ -di-neutron clustering configuration where the two valence neutrons are strongly correlated becomes important.

We can intuitively interpret this behavior as follows: when the spin-orbit is weak enough, the two valence neutrons form di-neutron, in which the attractive interaction between them strongly contributes. However, when the spin-orbit interaction significantly acts and becomes more important, the di-neutron is broken and each valence neutron rotates around the core in opposite direction with definite  $K$ -values. Note that the spin-orbit interaction does not act to di-neutron with  $S = 0$ . This is close to  $jj$ -coupling picture and axial symmetry of the system is restored.

This situation can be interpreted also from nuclear  $SU_3$  model. At the  $SU_3$  limit (parameters  $a$ ,  $b$ , and  $d \rightarrow 0$ ),  $\Phi((3/2^-)^2)$  (dominant configuration of  $2_1^+$ ) and  $\Phi(3/2^- 1/2^-)$

(dominant configuration of  $2_2^+$ ) correspond to linear combinations of two  $SU_3$  configurations:  $(n_x, n_y, n_z) = (2, 0, 4)$ ,  $(\lambda, \mu) = (2, 2)$  and  $(n_x, n_y, n_z) = (1, 1, 4)$ ,  $(\lambda, \mu) = (3, 0)$  ( $n_z = 4$  is due to the  $\alpha$ -clusters along the  $z$ -axis). This is because, the valence neutrons in  $3/2^-$  and  $1/2^-$  are expressed as linear combinations of  $p$ -orbitals along the  $x$ - and  $y$ -direction. Here, the spin-orbit interaction determines the mixing ratio of the two  $SU_3$  representations. When it is strong enough, since the  $jj$ -coupling picture works well, these two configurations are mixed to the almost same amount. However, when the spin-orbit interaction is weakened, the binding-energy gain due to the mixing amplitudes changes. Here, the  $(\lambda, \mu) = (2, 2)$  configuration, which is a di-neutron configuration, becomes much more important than the  $(\lambda, \mu) = (3, 1)$  configuration. This means that a triaxial deformation is induced when the spin-orbit interaction becomes weaker.

Next, we examine the magnetic dipole moment as a probe to determine the strength of the spin-orbit interaction. In Table III, the magnetic dipole moments of these two  $2^+$  states are listed, and we predict  $\mu = 0.72\mu_N$  and  $0.48\mu_N$  for the first and the second  $2^+$  states, respectively. Unfortunately, the dependence of the total magnetic moment of these states with respect to the spin-orbit strength is rather monotonic. However, each component has a significant dependence. In Table III, proton-orbital part and neutron-spin part are also listed (neutron-orbital part is of course zero, and proton-spin part also becomes zero due to the assumption of the  $\alpha$ -clusters).

As for the proton-orbital part, using the original interaction ( $V_0^{ls} = 2000$  MeV,  $M = 0.6$ ),  $2_1^+$  is calculated to have a larger value than  $2_2^+$ : the  $2_1^+$  state has  $1.13 \mu_N$  and the  $2_2^+$  state has  $0.46 \mu_N$ . The  $2_1^+$  state is mainly of  $K = 0$ , and therefore the rotation of the  $\alpha$ - $\alpha$  core is the main source of the angular momentum ( $J = 2$ ). However, in the case of  $2_2^+$ , since the valence neutrons already have  $K = 2$ , the rotation of  $\alpha$ - $\alpha$  is not necessary to construct  $J = 2$ , and hence the proton-orbital part is smaller than  $2_1^+$ . These values depend on the strength of the spin-orbit interaction. With decreasing spin-orbit strength, the difference of proton-orbital part between these two states becomes smaller due to the increase of the  $K$ -mixing effect between the two  $2^+$  configurations, which we discussed. When the strength of the spin-orbit interaction is  $V_0^{ls} = 1500$  MeV,  $2_1^+$  has  $1.04 \mu_N$  and  $2_2^+$  has  $0.65 \mu_N$ . As for the neutron-spin part, in  $V_0^{ls} = 2000$  MeV case (original interaction),  $2_1^+$  has  $-0.41 \mu_N$  and  $2_2^+$  has  $-0.04 \mu_N$ . This result suggests that the  $2_1^+$  state has both spin-singlet and spin-triplet components of the valence neutrons. The  $2_2^+$  state is dominated by the spin-singlet component. In  $2_2^+$ , one of the valence neutrons repulsively feels the spin-orbit interaction, and when the two valence neutrons construct spin-singlet, it helps to reduce the contribution of the repulsive spin-orbit interaction. This is the main reason for the smaller neutron-spin part in  $2_2^+$ . On the other hand, if we use weaker spin-orbit strength, the difference of neutron-spin part between the two  $2^+$  states becomes much smaller. When the strength of the spin-orbit interaction is  $V_0^{ls} = 1000$  MeV,  $2_1^+$  has  $-0.13 \mu_N$  and  $2_2^+$  has  $-0.12 \mu_N$ .

Finally, we comment that the  $K$ -mixing effect is also important for the  $4^+$  states. The  $4^+$  state with  $K = 0$  at  $-47.6$  MeV in Fig. 2 becomes  $-50.0$  MeV after the  $K$ -mixing, and the  $4^+$  state with  $K = 2$  at  $-46.1$  MeV is pushed up to  $-43.5$  MeV. The first  $4^+$  state has the squared overlap of 0.78 with the  $K = 0$  while 0.63 with the  $K = 2$  state (here,  $K = 0$  and  $K = 2$  are not orthogonal). Therefore, the first  $4^+$  state has almost equal contribution of the  $K = 0$  and the  $K = 2$  basis states. This is because, in the case of  $4^+$ , the angular momentum vector with  $K = 0$  and  $K = 2$  are not necessary to be spatially orthogonal,

different from the case of  $2^+$ . Therefore, the  $K$ -mixing for the  $4^+$  state of  $^{10}\text{Be}$  is very strong, and the electro-magnetic transition probability among the yrast band deviates from a simple rigid-body picture. The  $B(\text{E}2: 4_1^+ \rightarrow 2_1^+)$  value is calculated to be  $11.1 e^2\text{fm}^4$ , even smaller than the  $B(\text{E}2: 2_1^+ \rightarrow 0_1^+)$  value of  $11.8 e^2\text{fm}^4$ , and the  $\frac{B(\text{E}2: 4_1^+ \rightarrow 2_1^+)}{B(\text{E}2: 2_1^+ \rightarrow 0_1^+)}$  ratio of 0.94 much deviates from the rigid-body limit of 1.43. If we restrict the model space to  $K = 0$ , then the  $B(\text{E}2: 4_1^+ \rightarrow 2_1^+)$  becomes  $14.7 e^2\text{fm}^4$ , and the ratio  $\frac{B(\text{E}2: 4_1^+ \rightarrow 2_1^+)}{B(\text{E}2: 2_1^+ \rightarrow 0_1^+)}$  of 1.18 becomes closer to 1.43. In nuclear  $SU_3$  model, the  $4^+$  states with  $K = 0$  ( $(\lambda, \mu) = (2, 2)$ ) and  $K = 2$  ( $(\lambda, \mu) = (3, 1)$ ) become the same representation. This character partially remains as a strong  $K$ -mixing effect in the present MO model.

#### IV. SUMMARY AND CONCLUSION

We have applied the  $\alpha+\alpha+n+n$  model to  $^{10}\text{Be}$  and discussed the triaxial deformation of this nucleus. The orbits for the valence neutrons have been introduced based on the molecular orbit (MO) model. In the present model, the spatially extended motion of the valence neutrons around the  $\alpha$ -clusters are described by linear combinations of Gaussians, and the centers of the Gaussians are variationally determined.

The calculated energy levels show the appearance of two band structures, which have dominantly  $K = 0$  and  $K = 2$  components, when the two valence neutrons occupy  $K^\pi = 3/2^-$  or  $K^\pi = 1/2^-$  orbits. The first  $2^+$  state has the squared overlap with the  $K = 0$  state by 0.96, and the second  $2^+$  state has the squared overlap with the  $K = 2$  state by 0.92. Since the second  $2^+$  state has the component of  $K = 0$  by 8%, the electro-magnetic transition from the  $2_1^+$  state (mainly  $K = 0$ ) to the  $2_2^+$  state (mainly  $K = 2$ ) is allowed ( $3.99 e^2\text{fm}^4$ ). Using Davydov-Filippov model [12], we estimated the triaxiality for the  $2^+$  state. The ratio  $\frac{B(\text{E}2: 2_2^+ \rightarrow 2_1^+)}{B(\text{E}2: 2_1^+ \rightarrow 0_1^+)}$  calculated with the Davidov-Filippov model and our model coincide around  $\gamma = 19^\circ$ , and  $B(\text{E}2)$  ratio  $\frac{B(\text{E}2: 2_2^+ \rightarrow 0_1^+)}{B(\text{E}2: 2_1^+ \rightarrow 0_1^+)}$  indicates  $\gamma = 17^\circ \sim 22^\circ$ . Originally, the  $\alpha$ - $\alpha$  core is introduced to be of axial symmetry. However, because of the recoil effect of the valence neutrons, the charge distribution deviates from the axial symmetry, and the system becomes triaxial. We also discussed the triaxial deformation by artificially weakening the spin-orbit interaction. With decreasing spin-orbit interaction, the orbits of the valence neutrons deviate from the  $jj$ -coupling limit, and the di-neutron configuration becomes important. Here, the system becomes 3 body-like and the  $B(\text{E}2: 2_2^+ \rightarrow 2_1^+)$  value drastically increases.

Similar di-neutron component is discussed in weakly bound systems with the so-called halo structure. For example, in  $^6\text{He}$ , in addition to the shell model-like space, the model space of di-neutron+ $^4\text{He}$  has been shown to be important [28]. This means that a locally-correlated di-neutron wave function is important for the description of the valence neutrons with small binding energy and spatially extended distribution. It is consistent with our discussion on the effect of varying the strength of the spin-orbit interaction. Namely, when the valence neutrons with low-binding energies have halo structure, the contribution of the spin-orbit interaction between the core and the valence neutrons becomes weak. Here, the valence neutrons construct a di-neutron pair with spin singlet, by which they can increase the spatial overlap between them and the contribution of the attractive interaction. Therefore, it is very challenging to explore the triaxial deformations in  $^{12}\text{Be}$  and  $^{14}\text{Be}$ , which have weakly

bound neutrons and also deformed cores.

The authors thank members of Nuclear Theory group in University of Tokyo and RI beam science laboratory in RIKEN for discussions and encouragements. They also thank Dr. I. Kumagai-Fuse for her help. One of the authors (N.I) thanks Prof. R. Lovas, Prof. W. von Oertzen, Prof. H. Horiuchi, Prof. K. Katō, and Dr. Y. Kanada-En'yo for fruitful discussions. This work is supported in part by Grant-in-Aid for Scientific Research (13740145) from the Ministry of Education, Science and Culture.

## REFERENCES

- [1] H. Iwasaki *et al.*, Phys. Lett. **B481**, 7 (2000).
- [2] H. Iwasaki *et al.*, Phys. Lett. **B491**, 8 (2000).
- [3] A. Navin *et al.*, Phys. Rev. Lett. **85**, 266 (2000).
- [4] A. A. Korscheninnikov *et al.* Phys. Lett. **B343**, 53 (1995).
- [5] N. Soić *et al.*, Eurohys. Lett, 34(1), 7 (1996).
- [6] M. Freer *et al.*, Phys. Rev. Lett. **82**, 1383 (1999).
- [7] M. Freer *et al.*, Phys. Rev. **C63**, 034301 (2001).
- [8] N. Itagaki and S. Okabe, Phys. Rev. C **61** 044306, (2000).
- [9] N. Itagaki, S. Okabe, and I. Ikeda, Phys. Rev. **C62**, 034301 (2000).
- [10] N. Itagaki, S. Okabe, K. Ikeda, and I. Tanihata, Phys. Rev. C **64** 014301, (2001).
- [11] M. Harvey and F. C. Khanna, Nuclear Spectroscopy and Reactions, Part D, Models of Light Nuclei, Ed. by J. Cerny, (Academic Press Inc., New York, 1975), 69.
- [12] A.S. Davydov and G.F. Filippov, Nucl. Phys. 8, 237 (1958).
- [13] N. Curtis *et al.*, submitted to Phys. Rev. C
- [14] Y. Abe, J. Hiura, and H. Tanaka, Prog. Theor. Phys. **49**, 800 (1973).
- [15] H. Furutani, H. Kanada, T. Kaneko, S. Nagata, H. Nishioka, S. Okabe S. Saito, T. Sakuda and M. Seya, Prog. Theor. Phys. Suppl. 68, 193 (1980).
- [16] M. Seya, M. Kohno and S. Nagata, Prog. Theor. Phys. 65, 204 (1981).
- [17] Y. Kanada-En'yo, H. Horiuchi and A.Doté, Phys. Rev. **C60**, 064304 (1999).
- [18] Y. Ogawa, K. Arai, Y. Suzuki, and K. Varga, Nucl. Phys. **A673**, 122 (2000).
- [19] Y. Kanada-En'yo and H. Horiuchi, Prog. Theor. Phys. 93, 115 (1995).
- [20] Y. Kanada-En'yo, H. Horiuchi and A. Ono, Phys. Rev. **C52**, 628 (1995).
- [21] Y. Kanada-En'yo and H. Horiuchi Phys. Rev. **C52**, 647 (1995).
- [22] A. Doté, H. Horiuchi and Y. Kanada-En'yo, Phys. Rev. **C56**, 1844 (1997).
- [23] A. Ono, H. Horiuchi, T. Maruyama and A. Ohnishi, Prog. Theor. Phys. 87 1185, (1992); Phys. Rev. Lett. 68 2898, (1992).
- [24] A.B. Volkov Nucl. Phys. 74, 33 (1965).
- [25] N. Yamaguchi, T. Kasahara, S. Nagata and Y. Akaishi, Prog. Theor. Phys. 62 1018 (1979)
- [26] S. Okabe and Y. Abe, Prog. Theor. Phys. 61, 1049 (1979).
- [27] V. Werner, N. Pietralla, P. von Brentano, R.F. Casten, and R.V. Jolos, Phys. Rev. **C61**, 021301(R) (2000).
- [28] S. Aoyama, S. Mukai, K. Katō, and K. Ikeda, Prog. Theor. Phys. **93**, 99 (1995).

## FIGURES

FIG. 1. The intrinsic density of  $\Phi((3/2^-)^2)$  ((a):  $xz$ -plane, (b):  $xy$ -plane), where the  $\alpha$ - $\alpha$  distance is chosen to be optimal 3 fm.

FIG. 2. The calculated energy levels of  $^{10}\text{Be}$ . The left and the middle column show the levels calculated with the constraints of  $K = 0$  and  $K = 2$ . The right column shows the calculated energy levels after  $K$ -mixing. The calculated  $\alpha+\alpha+n+n$  threshold energy ( $-55.0$  MeV) is shown as the dashed line. Experimentally, the  $2_1^+$  and the  $2_2^+$  states are observed at  $E_x = 3.3$  MeV and  $E_x = 5.9$  MeV, respectively.

FIG. 3. B(E2) ratios  $\frac{B(E2: 2_2^+ \rightarrow 2_1^+)}{B(E2: 2_1^+ \rightarrow 0_1^+)}$  (solid line) and  $\frac{B(E2: 2_2^+ \rightarrow 0_1^+)}{B(E2: 2_1^+ \rightarrow 0_1^+)}$  (dotted line), as a function of  $\gamma$  (degree). Our results of 0.34 and 0.059 cross with Davydov-Filippov model around  $15^\circ \sim 20^\circ$ .

TABLES

TABLE I. The values of  $a$ ,  $b$  and the intrinsic energy as a function of the  $\alpha$ - $\alpha$  distance. Parameter  $a$  for the spin-up and the spin-down valence neutrons  $a_1$  and  $a_2$ , respectively, and parameter  $b$  for them is  $b_1$  and  $b_2$ . The wave function of  $^{10}\text{Be}$  is  $\Phi((3/2^-)^2)$  (upper panel),  $\Phi((1/2^-)^2)$  (middle panel), and  $\Phi(3/2^-, 1/2^-)$  (lower panel).

$\alpha$ - $\alpha$ (fm)	$a_1 = a_2$ (fm)		$b$ (fm)		intrinsic (MeV)
2	1.09		0.99		-52.09
3	1.39		1.08		-50.91
4	1.71		1.35		-44.64
5	2.12		1.53		-38.04

$\alpha$ - $\alpha$ (fm)	$a_1 = a_2$ (fm)		$b$ (fm)		intrinsic (MeV)
2	1.33		2.05		-38.06
3	1.49		2.11		-39.30
4	1.63		2.21		-35.42
5	1.89		2.35		-30.34

$\alpha$ - $\alpha$ (fm)	$a_1$ (fm)	$a_2$ (fm)	$b_1$ (fm)	$b_2$ (fm)	intrinsic (MeV)
2	1.12	1.18	0.83	1.87	-50.20
3	1.33	1.37	1.12	1.94	-49.81
4	1.66	1.59	1.40	2.09	-44.16
5	2.05	2.36	1.59	2.23	-37.79

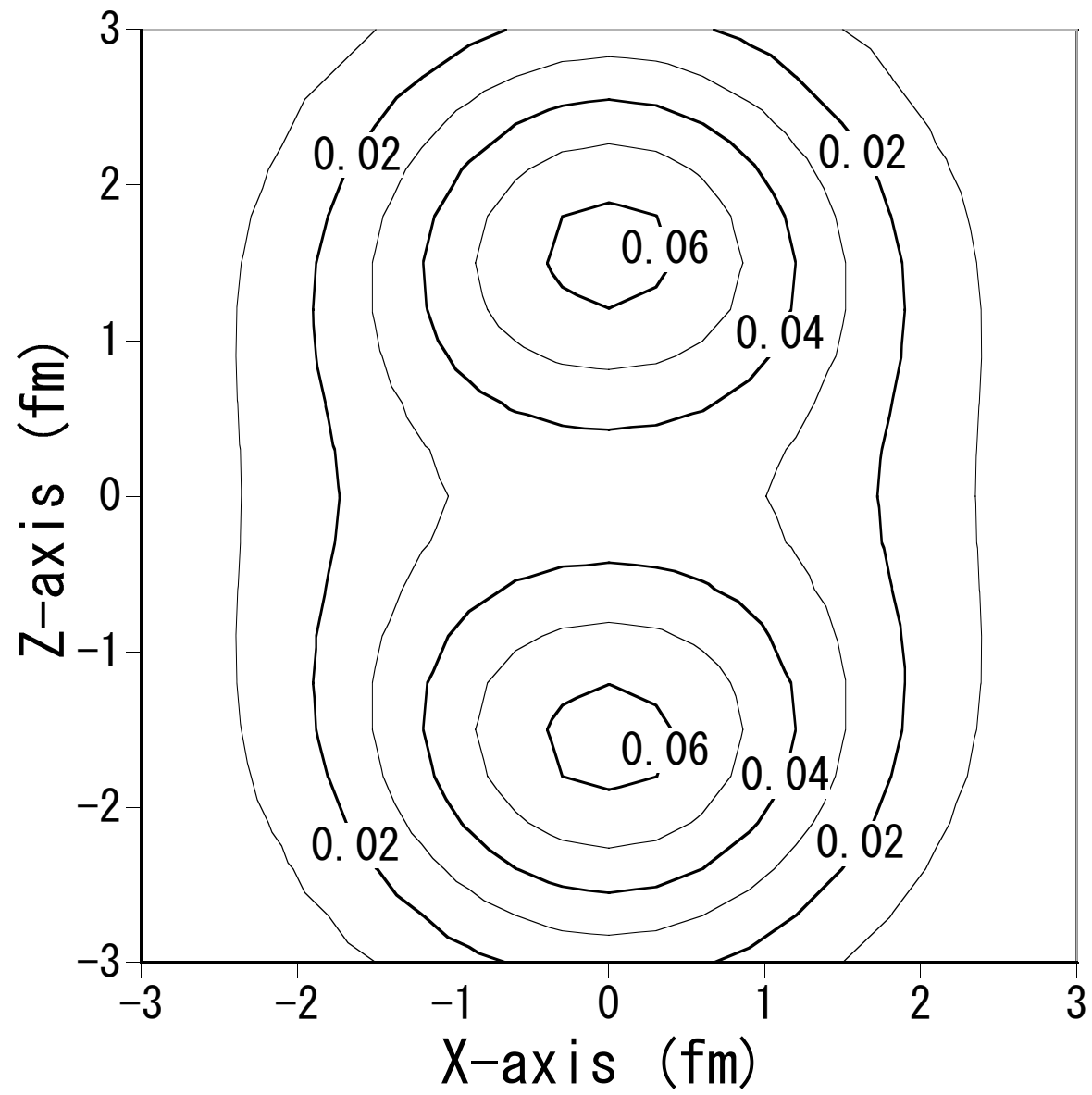
TABLE II. The electro-magnetic transition probability (B(E2)) in  $^{10}\text{Be}$  after the  $K$ -mixing. All units are  $e^2\text{fm}^4$ .

B(E2: $2_1^+ \rightarrow 0_1^+$ )	11.8 (Exp. $10.04 \pm 1.2$ )
B(E2: $2_2^+ \rightarrow 0_1^+$ )	0.70
B(E2: $2_1^+ \rightarrow 2_2^+$ )	3.99
B(E2: $4_2^+ \rightarrow 2_1^+$ )	11.1

TABLE III. The electro-magnetic transition probability (B(E2)) from first  $2^+$  state to second  $2^+$  calculated by changing the strength of the spin-orbit interaction ( $V_0^{ls}$ ). The Majorana parameter ( $M$ ) for the central interaction is also changed to keep the calculated binding energy constant. The original interaction is  $V_0^{ls} = 2000$  MeV and  $M = 0.6$ . Magnetic dipole moment is also predicted.  $\mu(pl)$  and  $\mu(ns)$  represent proton-orbital part and neutron-spin part, respectively.

$V_0^{ls}$ (MeV)	1000	1500	2000	2500
$M$	0.58	0.59	0.60	0.61
$0_1^+$ (MeV)	-60.48	-60.38	-60.51	-60.75
$2_1^+$ (MeV)	-57.69	-57.30	-57.26	-57.33
$2_2^+$ (MeV)	-56.71	-55.78	-54.88	-53.93
B(E2: $2_1^+ \rightarrow 2_2^+$ ) ( $e^2\text{fm}^4$ )	17.53	9.53	3.99	2.20
$\mu$ ( $2_1^+$ ) ( $\mu_N$ )	0.57	0.73	0.72	0.69
( $\mu(pl)$ , $\mu(ns)$ )	(0.70, -0.13)	(1.04, -0.30)	(1.13, -0.41)	(1.16, -0.48)
$\mu$ ( $2_2^+$ ) ( $\mu_N$ )	0.91	0.59	0.48	0.43
( $\mu(pl)$ , $\mu(ns)$ )	(1.03, -0.12)	(0.65, -0.06)	(0.51, -0.04)	(0.46, -0.03)

(a)



(b)

